LCDR regulates the integrity of lysosomal membrane by hnRNP K–stabilized *LAPTM5* transcript and promotes cell survival

Xiwang Yang[a,b,c,1], Ya Wen[a,c,1], Shaomin Liu[d,1], Liqiang Duan[c], Tongfeng Liu[a,b], Zhou Tong[c], Zhuo Wang[c], Yinmin Gu[b], Yibo Xi[c], Xiaodong Wang[b], Dingsan Luo[b], Ruobing Zhang[b], Yajuan Liu[c], Yang Wang[c], Tianyou Cheng[c], Siyuan Jiang[b], Xiaofeng Zhu[a,c], Xiaohui Yang[b], Yongbo Pan[c], Shuwen Cheng[e], Qinong Ye[f], Jinfei Chen[g,2], Xiaoding Xu[d,2], and Shan Gao[b,c,h,2]

[a]Medical School of Guizhou University, Guiyang 550025, China; [b]CAS Key Laboratory of Bio-Medical Diagnostics, Suzhou Institute of Biomedical Engineering and Technology, Chinese Academy of Sciences, Suzhou 215163, China; [c]Shanxi Academy of Advanced Research and Innovation, Taiyuan 030032, China; [d]Guangdong Provincial Key Laboratory of Malignant Tumor Epigenetics and Gene Regulation, Medical Research Center, Sun Yat-sen Memorial Hospital, Sun Yat-sen University, Guangzhou 510120, China; [e]Cancer Center, Taikang Xianlin Drum Tower Hospital, Nanjing University School of Medicine, Nanjing 210046, China; [f]Department of Medical Molecular Biology, Beijing Institute of Biotechnology, Collaborative Innovation Center for Cancer Medicine, Beijing 100850, China; [g]Department of Oncology, The First Affiliated Hospital of Wenzhou Medical University, Wenzhou 325000, China; and [h]Zhongda Hospital, Southeast University, Nanjing 210096, China

Edited by Ling-Ling Chen, Chinese Academy of Sciences Center for Excellence in Molecular Cell Science, Shanghai, China; received June 12, 2021; accepted December 2, 2021 by Editorial Board Member Louise T. Chow

Lysosome plays important roles in cellular homeostasis, and its dysregulation contributes to tumor growth and survival. However, the understanding of regulation and the underlying mechanism of lysosome in cancer survival is incomplete. Here, we reveal a role for a histone acetylation–regulated long noncoding RNA termed *lysosome cell death regulator* (*LCDR*) in lung cancer cell survival, in which its knockdown promotes apoptosis. Mechanistically, *LCDR* binds to heterogenous nuclear ribonucleoprotein K (hnRNP K) to regulate the stability of the *lysosomal-associated protein transmembrane 5* (*LAPTM5*) transcript that maintains the integrity of the lysosomal membrane. Knockdown of *LCDR*, hnRNP K, or LAPTM5 promotes lysosomal membrane permeabilization and lysosomal cell death, thus consequently resulting in apoptosis. LAPTM5 overexpression or cathepsin B inhibitor partially restores the effects of this axis on lysosomal cell death in vitro and in vivo. Similarly, targeting *LCDR* significantly decreased tumor growth of patient-derived xenografts of lung adenocarcinoma (LUAD) and had significant cell death using nanoparticles (NPs)-mediated systematic short interfering RNA delivery. Moreover, *LCDR*/hnRNP K/LAPTM5 are up-regulated in LUAD tissues, and coexpression of this axis shows the increased diagnostic value for LUAD. Collectively, we identified a long noncoding RNA that regulates lysosome function at the posttranscriptional level. These findings shed light on *LCDR*/hnRNP K/LAPTM5 as potential therapeutic targets, and targeting lysosome is a promising strategy in cancer treatment.

LCDR | hnRNP K | LAPTM5 | lysosome | apoptosis

Lysosome is involved in cellular homeostasis in physiology, and its dysregulation has been linked to various human diseases, including cancer (1, 2). The functional alterations of lysosome are able to drive cancer growth and survival or result from a consequence of cancer (2–4). However, the underlying mechanism in which the lysosomes promote the survival of cancer cells remains poorly understood.

Long noncoding RNAs (lncRNAs) are noncoding RNAs with length longer than 200 nucleotides (nt) whose dysregulation is associated with cancer hallmarks (5, 6). lncRNAs play diverse roles in regulating gene expression by interacting with DNA, RNA, proteins, and/or their combination, including the heterogeneous nuclear ribonucleoprotein (hnRNP) family (7–10). The interaction between lncRNAs and hnRNPs regulates multiple aspects of RNAs including alternative splicing, RNA stability, and translation to drive cancer growth and survival (11). Whether lncRNAs and/or hnRNPs are involved in lysosome-mediated cancer survival is not elucidated.

Cancer is driven as a result of a series of genetic and epigenetic alterations. Epigenetic alterations include histone modifications, such as acetylation, methylation, etc. (12). The interplay between histone modification and lncRNAs is one of key epigenetic events in cancer (13). In this study, we identified a histone acetylation–regulated (HAR) lncRNA (ENSG00000273148) binding to heterogenous nuclear ribonucleoprotein K (hnRNP K) to maintain the integrity of lysosomal membrane by stabilizing *lysosomal-associated protein transmembrane 5* (*LAPTM5*) stability, thus preventing lysosomal cell death (LCD) and promoting cancer cell survival, so we termed this lncRNA *lysosome cell*

Significance

Here, we report that the long noncoding RNA *lysosome cell death regulator* (*LCDR*) mediates the survival of cancer cells, counteracting the effects of apoptosis triggered by lysosomal cell death pathways. Mechanistically, *LCDR*, as a cofactor for heterogenous nuclear ribonucleoprotein K (hnRNP K) to potentiate the stabilization of lysosomal membrane protein lysosomal-associated protein transmembrane 5 (LAPTM5), prevents lysosomal membrane permeabilization and promotes cancer cell survival. Clinically, *LCDR*, hnRNP K, and LAPTM5 are significantly up-regulated in lung adenocarcinoma (LUAD) patients. Targeting *LCDR* via nanoparticles-mediated RNA interference technology increases cell death in vitro and inhibits the growth of patient-derived xenografts of LUAD in vivo. Our study demonstrates that *LCDR* contributes to cancer pathology by regulating *LCDR*-mediated apoptosis.

Author contributions: X.Y., Y. Wen, and S.G. designed research; X.Y., Y. Wen, T.L., Z.T., Z.W., Y.G., X.W., Y.L., Y. Wang, T.C., S.J., X.Z., X.Y., and Y.P. performed research; S.L., D.L., R.Z., and X.X. contributed new reagents/analytic tools; X.Y., L.D., Y.G., Y.X., S.C., and S.G. analyzed data; and Y.G., Q.Y., J.C., and S.G. wrote the paper.

The authors declare no competing interest.

This article is a PNAS Direct Submission. L.-L.C. is a guest editor invited by the Editorial Board.

[1]X.Y., Y. Wen, and S.L. contributed equally to this work.

[2]To whom correspondence may be addressed. Email: jinfeichen@sohu.com, xuxiaod5@mail.sysu.edu.cn, or gaos@sibet.ac.cn.

This article contains supporting information online at http://www.pnas.org/lookup/suppl/doi:10.1073/pnas.2110428119/-/DCSupplemental.

Published January 28, 2022.

death regulator (*LCDR*). Collectively, these findings shed light on the key roles of the *LCDR*/hnRNP K/LAPTM5 axis on lysosome and cancer, providing potential diagnostic and/or therapeutic targets for lung cancer.

Results

***LCDR* Is Expressed in Cancer Cells.** The regulation of gene expression by histone acetylation is balanced between the activities of histone acetyltransferases and histone deacetylases (HDACs) (14). To explore HAR lncRNAs in lung cells, we analyzed the expression profiles of both BSEA-2B immortalized lung epithelial cells and NCI-H1299 lung cancer cells treated using the HDAC inhibitor Trichostatin A (TSA), revealing changes in differentially expressed genes (DEGs) including protein coding genes and lncRNAs (Dataset S1 and *SI Appendix*, Fig. S1 *A–D*). Kyoto Encyclopedia of Genes and Genomes (KEGG) enrichment analysis revealed that these overlapped DEGs were enriched in the "Transcriptional misregulation in cancer" pathway (*SI Appendix*, Fig. S1*E*), supporting the roles of histone acetylation in the transcriptional regulation of gene expression (12). To further identify deregulated HAR lncRNAs in cancer, we analyzed the aberrantly expressed lncRNAs in the various cancer types, including lung, head and neck, liver, cholecyst, stomach, and kidney, that our laboratory focused on. Using The Cancer Genome Atlas database, we identified 24 commonly up-regulated lncRNAs among these cancer types and the two lung cell lines (Datasets S2 and S3 and *SI Appendix*, Fig. S1 *F* and *G*). It is well known that H4K16ac and H3K27ac are conserved marks for gene transcription (14), but we found that TSA inhibitors were able to increase H3K27ac expression globally but not H4K16ac in lung cell lines (*SI Appendix*, Fig. S1*H*). We further integrated H3K27ac chromatin immunoprecipitation (ChIP) sequence data and found that promoters of seven up-regulated lncRNAs were enriched with H3K27ac peaks (Dataset S4 and *SI Appendix*, Fig. S2 *A* and *B*). Notably, we noticed an uncharacterized lncRNA (ENSG00000273148; termed *LCDR*), which was chosen for further study. After TSA treatment, qRT-PCR analysis revealed that *LCDR* expression was increased (*SI Appendix*, Fig. S2 *C–E*), and the ChIP qRT-PCR–verified promoter of *LCDR* was increased in H3K27ac enrichment (*SI Appendix*, Fig. S2 *F–H*). Altogether, these data suggest *LCDR* is a potential functional HAR lncRNA that is up-regulated in cancer.

To study the potential oncogenic role of *LCDR* in lung cancer cells, we first performed 5′ and 3′ rapid amplification of cDNA ends and found that *LCDR* was a 2,013-nt transcript with one exon (*SI Appendix*, Fig. S3*A* and Table S1), the expected size of which was verified by northern blot (*SI Appendix*, Fig. S3*B*). *LCDR* is a noncoding transcript with analysis of the Coning Potential Calculator (*SI Appendix*, Fig. S3*C*). Cellular fractionation assays and RNA fluorescence in situ hybridization (FISH) revealed that *LCDR* was mainly located in the nucleus of NCI-H1299 cells, which was further verified by short interfering RNA (siRNA)–mediated *LCDR* knockdown (KD) (*SI Appendix*, Fig. S3 *D* and *E*). Moreover, the expression levels (*SI Appendix*, Fig. S3*F*) and copy number (*SI Appendix*, Fig. S3*G*) of *LCDR* were higher in three lung cancer lines than the BSEA-2B cell line. Altogether, these results indicate that *LCDR* is expressed in lung cells.

To further define the molecular mechanism driving *LCDR* expression in lung cancer cells, we examined the region of *LCDR* gene in the Encyclopedia of DNA Elements (ENCODE), which revealed that seven epigenetic signatures, including H3K27ac, commonly associated with activation of transcription were enriched around the transcription starting site (TSS) of *LCDR* (*SI Appendix*, Fig. S3*H*); c-Jun was peaked in the promoter region of *LCDR*, suggesting that c-Jun is a potential transcriptional factor (*SI Appendix*, Fig. S4*A*). We, therefore, further confirmed the effects of c-Jun on *LCDR* expression. Overexpression (OE) of c-Jun increased and KD of c-Jun decreased *LCDR* expression in lung cancer cells (*SI Appendix*, Fig. S4 *B* and *C*). ChIP qRT-PCR analyses showed that c-Jun directly bound to the promoter of *LCDR* but not the promoter of U1 (*SI Appendix*, Fig. S4*D*). Moreover, two putative c-Jun binding sites (BSs) on upstream of the *LCDR* TSS were predicted based on c-Jun binding profiles of ENCODE (*SI Appendix*, Fig. S4*E*). Luciferase reporter assay showed that c-Jun OE increased the luciferase activity of the *LCDR* promoter wild-type reporter and mutated BS2 (mut2) reporter but not the mutated BS1 (mut1) reporter (*SI Appendix*, Fig. S4 *F* and *G*), suggesting that BS1 is the c-Jun BS. Moreover, ChIP qRT-PCR analyses revealed that c-Jun further increased the occupancy on the promoter of *LCDR* after TSA treatment (*SI Appendix*, Fig. S4*H*), suggesting that c-Jun is more accessible to the promoter of *LCDR* after TSA treatment. Taken together, these data suggest that *LCDR* is transcribed by c-Jun in lung cancer cells.

***LCDR*-Mediated Lung Cancer Cell Survival.** To explore the potential underlying role of *LCDR* on lung cancer cells, we used two short hairpin RNAs (shRNA) and two siRNAs that target the distinct sequences to knock down endogenous *LCDR* in NCI-H1299 cells (Fig. 1*A* and *SI Appendix*, Fig. S5*A*). *LCDR* silencing resulted in significantly decreased cell proliferation and colony formation (Fig. 1 *B* and *C* and *SI Appendix*, Fig. S5 *B* and *C*). Furthermore, we found that the *LCDR*-depleted cells exhibited morphological changes and characteristics of apoptosis, such as cell shrinkage, rounding, blebbing, and detachment (*SI Appendix*, Fig. S5 *D* and *E*). Also, annexin V apoptosis assay revealed that annexin V–positive cells were significantly higher in *LCDR*-depleted cells compared with the control cells (Fig. 1 *D* and *E* and *SI Appendix*, Fig. S5 *F* and *G*). Moreover, *LCDR* silencing cells were associated with the release of cytochrome *c* from mitochondria, activation of caspase-3, and cleavage of its substrate Poly(ADP-ribose) polymerase-1 (PARP-1) (Fig. 1 *F* and *G* and *SI Appendix*, Fig. S5 *H* and *I*). These data indicate that *LCDR* silencing leads to apoptosis of lung cancer cells. We also investigated the roles of *LCDR* on tumor growth in vivo. *LCDR* KD significantly inhibited in vivo xenograft tumor growth and mass of NCI-H1299 cells (Fig. 1 *H–J*). We further examined the cleaved caspase-3 levels by immunohistochemistry (IHC). Tumors from *LCDR* shRNA-transfected cells exhibited an increase in cleaved caspase-3 levels compared with the control cells (Fig. 1 *K* and *L*). Collectively, these data indicate that *LCDR* promotes lung cancer cell survival.

***LCDR* Interacts with hnRNP K.** Given that lncRNAs exert their functions mainly by binding to specific proteins (5), we performed an RNA pull-down assay followed with mass spectrometry to screen *LCDR*-interacting proteins, which revealed that hnRNP K is a putative *LCDR* binding protein (Fig. 2*A* and Dataset S5). hnRNP K is an RNA binding protein (RBP) and belongs to the hnRNP family (11, 15). We confirmed that hnRNP K was able to bind to *LCDR* (Fig. 2*B*). Furthermore, RNA immunoprecipitation (RIP) assay verified that hnRNP K was associated with *LCDR* but not the *U1* control (Fig. 2*C*). *LCDR* FISH followed by immunofluorescence of hnRNP K demonstrated the colocalization of *LCDR* and hnRNP K in the nucleus (Fig. 2*D*), further supporting their interaction.

To determine which region of *LCDR* is responsible for binding to hnRNP K, we first employed a truncated mapping strategy using in vitro–transcribed *LCDR* fragments to pull down the hnRNP K. Data revealed that the first fragment containing 1 to 500 nt was associated with hnRNP K similar to the full length of *LCDR* (Fig. 2*E*), suggesting that 1 to 500 nt are critical for the interaction of *LCDR* with hnRNP K. To further identify the specific site for binding to hnRNP K, we predicted the secondary

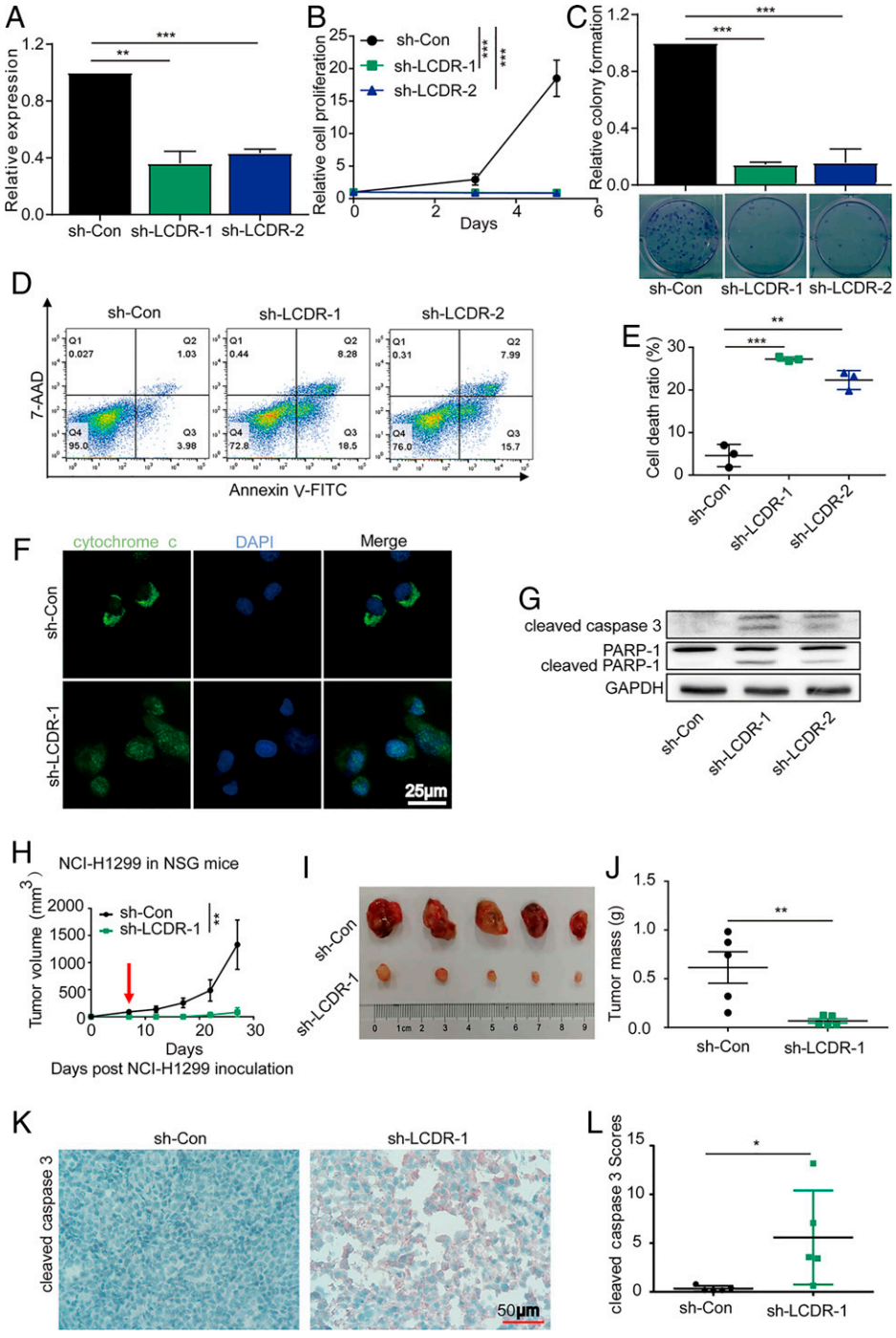

Fig. 1. The effects of *LCDR* KD on cell death. (*A*) The KD efficiency of *LCDR* was verified by qRT-PCR analysis of NCI-H1299 cells transfected with the indicated shRNAs for 48 h. sh-Con represents a negative control of short hairpin plasmids. (*B*) The Cell Titer-Glo Luminescent Cell Viability assay for the cell proliferation in NCI-H1299 cells transfected with the indicated shRNAs. (*C*) Representative images of the colony formation assay (*Lower*) and quantification data (*Upper*) for NCI-H1299 cells transfected with the indicated shRNAs. (*D* and *E*) Representative flow cytometry plots (*D*) and percentages (*E*) of the apoptosis of NCI-H1299 cells transfected with the indicated plasmids for 48 h. Cell apoptosis was measured by staining of Annexin V and 7-AAD. (*F*) Representative cytochrome *c* confocal images of NCI-H1299 cells transfected with the indicated plasmids. (Scale bar: 25 μm.) (*G*) Immunoblot analysis of the indicated proteins of NCI-H1299 cells transfected with the indicated plasmids. (*H*) Effects of NCI-H1299 cells transfected with the indicated plasmids on tumor growth in subcutaneously implanted NSG mice. The same number of cells was injected into the recipient mouse on day 0 as baseline and formed measurable tumors on day 7 (red arrow). (*I* and *J*) Tumor size (*I*) and mass (*J*) in NSG mice subcutaneously implanted with NCI-H1299 cells transfected with the indicated plasmids ($n = 5$). (*K* and *L*) Representative images of cleaved caspase-3 (*K*) and quantification of signal intensities (*L*) of tumor biospecimens in indicated xenografts ($n = 5$). 7-AAD, 7-aminoactinomycin D. DAPI, 4′,6-diamidino-2-phenylindole. GAPDH, glyceraldehyde-3-phosphate dehydrogenase. FITC, fluorescein isothiocyanate. Data present the mean ± SD. (Scale bar: 50 μm.) $^*P < 0.05$, Student's *t* test; $^{**}P < 0.01$, Student's *t* test; $^{***}P < 0.001$, Student's *t* test.

structure of this binding fragment using Mfold (16) and RNAfold (17), which revealed a single-stranded 217- to 225-nt polycytosine (poly[C]) site (Fig. 2 *F* and *G*). It has been reported that hnRNP K consists of three K homology (KH) domains with higher specificity of binding to the single-stranded poly(C) RNA site (18–20). We hypothesized that this poly(C) site is essential for hnRNP K binding and constructed a mutant containing the mutated poly(C) site (Fig. 2*G*). Consequently, the mutant completely abolished the binding of *LCDR* with hnRNP K (Fig. 2*H*). We further verified that hnRNP K bound to the probe containing this poly(C) site but not the mutant by electrophoretic mobility shift assay (EMSA) (Fig. 2*I*). Moreover, OE of *LCDR* increased and OE of *LCDR* mutant failed to increase the binding of hnRNP K (Fig. 2*J*). These data demonstrate that this poly(C) site is the specific BS of *LCDR* with hnRNP K. Next, we also determined the binding domains of hnRNP K with *LCDR* and generated a series of mutants with the deleted KH domain (Fig. 2 *K* and *L*). RIP assays demonstrated that *LCDR* bound to the KH1 domain of hnRNP K (Fig. 2*M*). Altogether, these data indicate that *LCDR* physically interacts with hnRNP K.

***LCDR* and hnRNP K Cooperate to Promote Cancer Cell Survival.** As shown the interaction between *LCDR* and hnRNP K, we hypothesized that hnRNP K may have the similar effects on cancer cell survival. We knocked down endogenous hnRNP K using two different siRNAs in NCI-H1299 cells (*SI Appendix*,

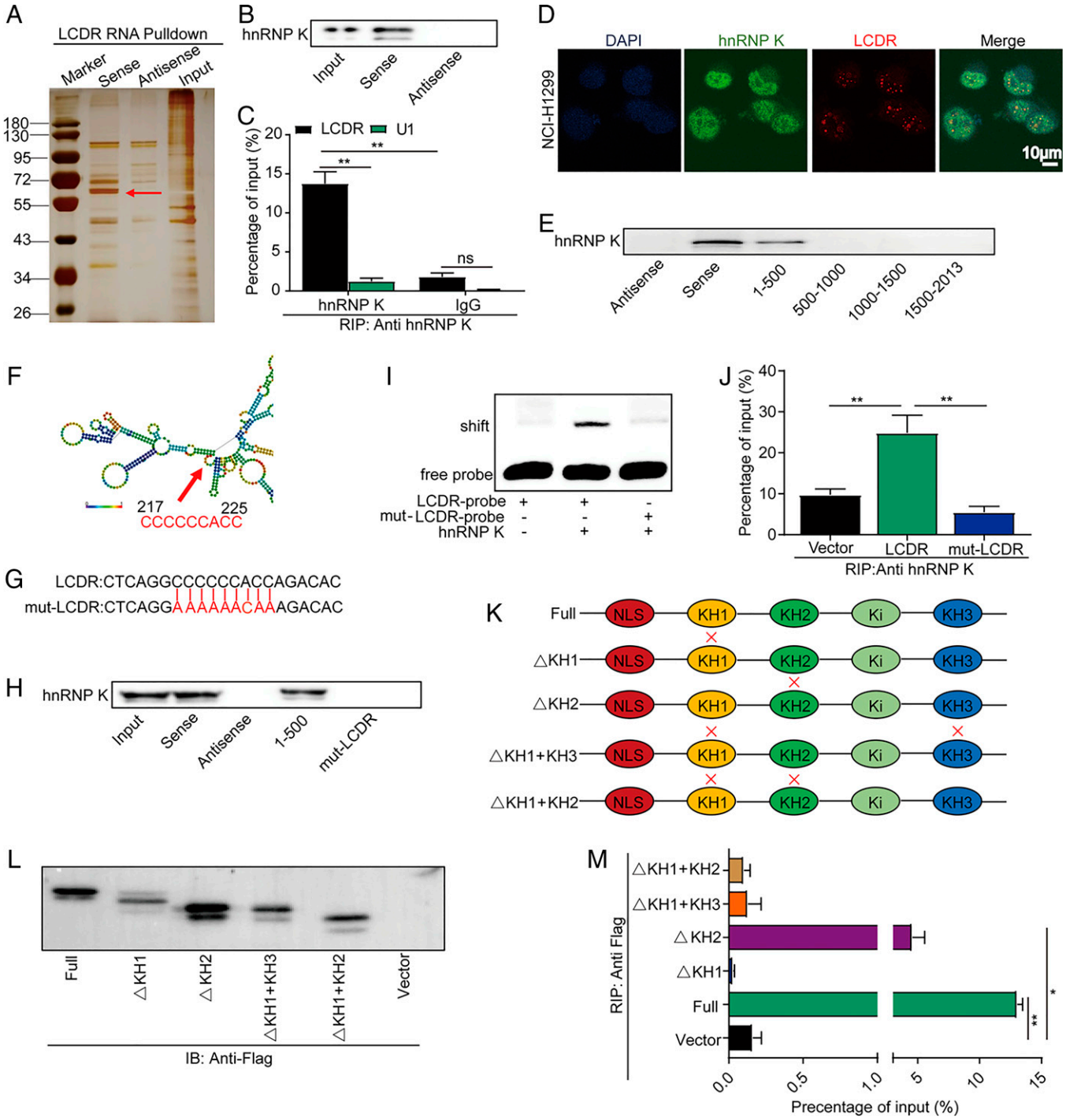

Fig. 2. *LCDR* directly binds with hnRNP K. (*A*) Silver staining of proteins by biotinylated sense and antisense *LCDR* pull down with total protein extracts from NCI-H1299 cells. The specific band is identified as hnRNP K (red arrow). (*B*) Immunoblot analysis of the association of hnRNP K with biotinylated *LCDR*. (*C*) RIP assays confirming the interaction between hnRNP K and *LCDR* in NCI-H1299 cells. (*D*) Confocal images showing the colocalization of *LCDR* and hnRNP K in NCI-H1299 cells. (Scale bar: 10 μm.) (*E*) RNA pull-down assay for the hnRNP K binding region of *LCDR* using the truncated mapping. (*F*) Secondary structure prediction of *LCDR* 1 to 500 nt showing a single-stranded poly(C) site. (*G*) Schematic diagram of the poly(C) mutation strategy. (*H*) Immunoblot showing the hnRNP K binding region in 1 to 500 nt of *LCDR*. (*I*) EMSA showing the specific interaction between hnRNP K and biotinylated *LCDR* probes. (*J*) The enrichment efficiency of *LCDR* by RIP assays using the hnRNP K antibody in *LCDR* OE and mut-*LCDR* cells. (*K–M*) Schematic representation of the hnRNP K functional domain and various truncated mutants with deleted domain (*K*). Immunoblot analysis using FLAG antibody (*L*) and RIP analysis for *LCDR* enrichment (*M*) in HEK293T cells transfected with the FLAG-tagged full-length or truncated hnRNP K constructs. DAPI, 4′,6-diamidino-2-phenylindole. ns, not significant. NLS, nuclear localization sequence. Ki, K-protein-interaction. mut, mutation. FLAG, FLAG tag peptide. Data present the mean ± SD. **P* < 0.05, Student's *t* test; ***P* < 0.01, Student's *t* test.

Fig. S6*A*), which led to significantly decreased cell proliferation and colony formation (*SI Appendix*, Fig. S6 *B* and *C*). Moreover, morphological changes, annexin V staining, cytochrome *c* staining, and cleaved caspase-3/PARP-1 showed similar effects in hnRNP K–depleted cells comparable with *LCDR*-depleted cells (*SI Appendix*, Fig. S6 *D–H*). Collectively, these data suggest hnRNP K is essential for survival of lung cancer cells.

To further characterize the molecular consequences of the *LCDR* and hnRNP K interaction, we performed qRT-PCR and immunoblot assays, which revealed that *LCDR* and hnRNP K failed to alter each other's expression level (*SI Appendix*, Fig. S7 *A–D*). Moreover, *LCDR* and hnRNP K KD did not affect each other's cellular localization and fluorescence intensity (*SI Appendix*, Fig. S7*E*). We next explored the role of the *LCDR*/hnRNP K axis on the survival effects of lung cancer cells and performed rescue experiments. Strikingly, *LCDR* KD abolished the cell proliferation effects elicited by the hnRNP K OE (*SI Appendix*, Fig. S7*F*). Conversely, hnRNP K KD abrogated the promoting effects of *LCDR* OE on cell proliferation (*SI Appendix*, Fig. S7*G*). Overall, these results suggest that *LCDR* and hnRNP K may cooperate to mediate cell survival in lung cancer.

hnRNP K has been implicated in apoptosis by regulating the various pro-/antiapoptotic molecules, so we examined the expression levels of pro-/antiapoptotic molecules that are involved in hnRNP K–mediated effects on cancer cell apoptosis (21, 22). Correspondingly, messenger RNA (mRNA) and protein levels of these pro-/antiapoptotic molecules were not significantly altered in both *LCDR*-depleted and hnRNP K–depleted cells (*SI Appendix*, Fig. S8), suggesting that the *LCDR*/hnRNP K axis regulates apoptosis via other signaling pathways.

***LCDR* and hnRNP K Regulate the Integrity of Lysosome.** Given that both *LCDR* and hnRNP K cooperate to regulate apoptosis and hnRNP K regulates gene expression via various mechanisms (15), we hypothesized that *LCDR* modulates hnRNP K–dependent gene regulation. We thus performed RNA-sequencing (RNA-seq) of both *LCDR* and hnRNP K KD cells and identified the common targets potentially regulated by *LCDR* and hnRNP K (Datasets S6 and S7 and *SI Appendix*, Fig. S9 *A–E*). We observed strong overlapping of DEGs in both *LCDR* and hnRNP K KD (Fig. 3 *A* and *B* and Dataset S8), suggesting a functional interaction between *LCDR* and hnRNP K. KEGG analysis of *LCDR* KD, hnRNP K KD, or the common DEGs revealed nine common signaling pathways, including lysosome (Fig. 3*C* and *SI Appendix*, Fig. S9 *C* and *F*). LCD, also known as lysosome-dependent cell death, is a type of regulated cell death mediated by hydrolytic enzymes that released into cytosol after lysosomal membrane permeabilization (LMP) (23–25). LCD may also amplify or initiate cell death signaling in the context of apoptosis, autophagy-dependent cell death, or ferroptosis (23), leading us to hypothesize that *LCDR*/hnRNP K may regulate LCD. We next validated the expression levels of five genes among top six common genes in the lysosome pathway (Fig. 3 *D–G*). Notably, it has been reported that LAPTM5 is expressed on the membrane of lysosome (26). Similar to the transcript levels, the protein levels of LAPTM5 were reduced in the KD of both *LCDR* and hnRNP K cells (*SI Appendix*, Fig. S10 *A* and *B*). Conversely, OE of *LCDR* and hnRNP K up-regulated LAPTM5 expression (*SI Appendix*, Fig. S10 *C–F*). Indeed, immunofluorescence showed that LAPTM5 colocalized with the lysosomal marker LAMP1 (*SI Appendix*, Fig. S10*G*). Furthermore, the colocalization of LAPTM5–green fluorescent protein (LAPTM5-GFP) and LAMP1 was observed in lung cancer cells (*SI Appendix*, Fig. S10*H*). These data demonstrate that LAPTM5 is expressed in lysosome and regulated by *LCDR*/hnRNP K.

Since LAPTM5 expression is regulated by the *LCDR*/hnRNP K axis, we hypothesized that LAPTM5 may have similar effects on cell survival. KD of LAPTM5 using two distinct siRNAs suppressed cell proliferation and colony formation (*SI Appendix*, Fig. S11 *A–C*). Effects of LAPTM5 KD on apoptosis recapitulated the effects of *LCDR*/hnRNP K KD, which were shown by morphological changes, annexin V staining, cytochrome *c* staining, and cleaved caspase-3/PARP-1 (*SI Appendix*, Fig. S11 *D–H*). Furthermore, we also explored the potential underlying roles of other lysosome genes (*ACP2*, *ARSB*, *ASAH1*, *HGSNAT*) on lung cancer cells. Strikingly, silencing of these genes using two distinct siRNAs did not lead to cell apoptosis (*SI Appendix*, Fig. S12), suggesting that LAPTM5 is only involved in apoptosis.

As we observed that the *LCDR*/hnRNP K/LAPTM5 axis shows the similar effects on cancer cell survival, we hypothesized that *LCDR*/hnRNP K/LAPTM5 regulates LCD via maintaining the integrity of lysosomal membrane. We performed the LysoTracker assay and found that the probes formed punctate staining patterns in control cells, while the probes dissipated throughout the cytosol in *LCDR*-/hnRNP K–/LAPTM5-depleted cells (Fig. 3*H*), suggesting that the lysosomes of these cells are permeabilized. Furthermore, in control cells, LAMP1 and cathepsin B (CTSB) were colocalized, while they show no association in *LCDR*/hnRNP K/LAPTM5 silencing cells (Fig. 3*H*), indicating that KD of the *LCDR*/hnRNP K/LAPTM5 axis results in LMP. Moreover, we observed partial permeabilization of the lysosomal membrane in *LCDR*/hnRNP K/LAPTM5 silenced cells using the scanning electronic microscope (Fig. 3*I*). Overall, these data demonstrate that the *LCDR*/hnRNP K/LAPTM5 axis regulates the integrity of lysosome membrane.

***LCDR* and hnRNP K Coordinate Cell Survival through LAPTM5.** Given the above findings, we thus determine whether LAPTM5 is a key downstream effector of the *LCDR*/hnRNP K axis promoting the survival of lung cancer cells. We next performed rescue experiments. As expected, the inhibitory effects of *LCDR*/hnRNP K KD either on both cell proliferation and colony formation or on cell death were partially rescued by LAPTM5 OE (Fig. 4 *A–D* and *SI Appendix*, Fig. S13 *A–F*). It has been shown that cathepsins play a major role in promoting LCD, and blocking cathepsin activity can prevent LCD (23). CA-074Me is highly a selective CTSB inhibitor (27); thus, we explored the blocked effects of CTSB release on cell death after *LCDR*/hnRNP K/LAPTM5 depletion. Strikingly, CA-074Me restored the cell death that was caused by *LCDR*/hnRNP K/LAPTM5 depletion, suggesting that the release of CTSB from lysosome regulates LCD in lung cancer cells (*SI Appendix*, Fig. S13 *G–L*). Furthermore, we also explored the role of LAPTM5 in *LCDR*/hnRNP K–mediated tumor growth in vivo. As expected, the inhibitory effects of *LCDR*/hnRNP K KD on xenograft tumor growth and mass of NCI-H1299 cells were partially rescued by LAPTM5 OE (Fig. 4 *E–G*). IHC staining of the tumor sections confirmed the decreased level of LAPTM5 and increased the cleaved caspase-3 level in *LCDR*/hnRNP K KD tumors (Fig. *4 H–J*). Collectively, these data demonstrate that *LCDR* and hnRNP K promote cell survival through LAPTM5.

hnRNP K Binds to *LAPTM5*. hnRNP K exerts functional roles mainly by binding to the target RNAs (5, 17). In order to determine whether hnRNP K binds to *LAPTM5*, we performed the integrated analysis on the RNA-seq data of *LCDR*/hnRNP K KD and two published hnRNP K RIP sequences and enhanced cross-linking immunoprecipitation sequencing (eCLIP-seq) data to identify the binding targets that were potentially regulated by *LCDR* and hnRNP K (Fig. 5*A* and Datasets S9–S11) (28, 29), which were enriched in the signaling pathways, including lysosome, using KEGG database analysis (Fig. 5*B*). *LAPTM5* rather than other lysosome pathway genes (*ACP2*, *ARSB*, *ASAH1*, and *HGSNAT*) was identified as an hnRNP K–bound transcript, and the gene-specific hnRNP K RIP qRT-PCR assays showed that

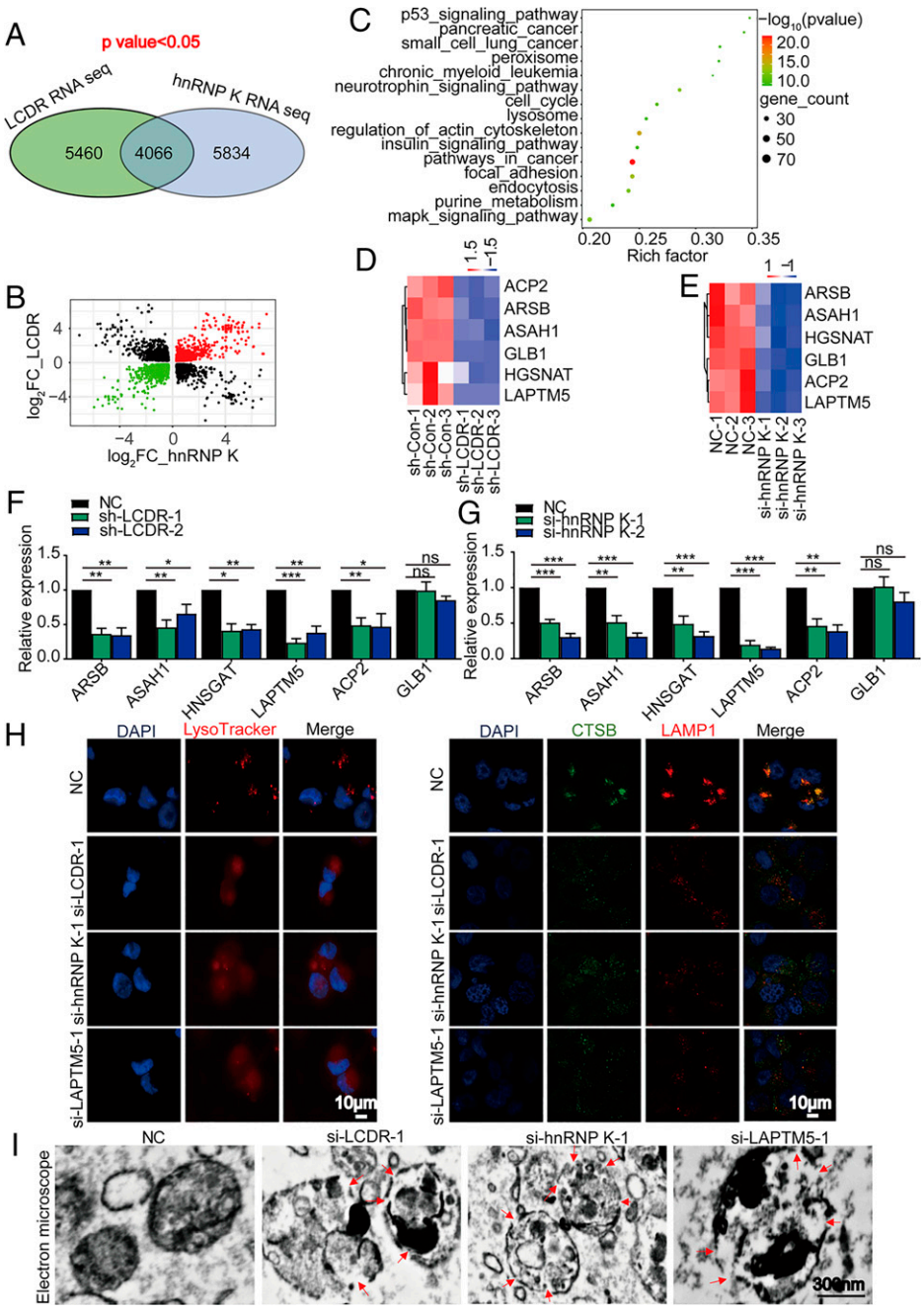

Fig. 3. *LCDR*/hnRNP K/LAPTM5 regulates lysosomal membrane permeability. (*A* and *B*) Venn diagram (*A*) and volcano plot (*B*) showing the overlapping DEGs between *LCDR* KD and hnRNP K KD RNA-seq data. DEGs were cut off using $P < 0.05$. Red or green dots represent commonly up-regulated or down-regulated genes, respectively (*B*). (*C*) The top 15 enriched KEGG pathways of the overlapping DEGs. (*D* and *E*) Heat map showing commonly dysregulated genes related to the lysosome pathway in the *LCDR* KD (*D*) and hnRNP K KD (*E*) RNA-seq. NC represents siRNA negative control. (*F* and *G*) qRT-PCR analysis of the relative expression levels of the indicated genes in the *LCDR* KD (*F*) and hnRNP K KD (*G*) NCI-H1299 cells. (*H*) Representative confocal images of lysoTracker (*Left*) and LAMP1 and CTSB (*Right*) localization in the *LCDR* KD, hnRNP K KD, and LAPTM5 KD NCI-H1299 cells. (Scale bars: 10 μm.) (*I*) Representative scanning electron microscope images of the lysosome of NCI-H1299 cells transfected with the indicated siRNAs. Red arrow points to permeabilization of the lysosomal membrane. FC, fold-change. DAPI, 4′,6-diamidino-2-phenylindole. These data are presented as mean ± SD from three independent experiments. ns, not significant, Student's *t* test. (Scale bar: 300 nm.) $*P < 0.05$, Student's *t* test; $**P < 0.01$, Student's *t* test; $***P < 0.001$, Student's *t* test.

hnRNP K only bound to *LAPTM5* (Fig. 5*C*). We further searched for the potentially hnRNP K–bound sites that were peak in both the 3′ untranslated region (UTR) and the coding sequence (CDS) in *LAPTM5* (Fig. 5*D*) (28, 29). We constructed luciferase reporters for the 3′ UTR and CDS of *LAPTM5*. OE of either *LCDR* or hnRNP K increased the activities of 3′ UTR but not CDS reporter, suggesting that hnRNP K binds to the 3′ UTR of *LAPTM5* (Fig. 5*E*). We further found a poly(C) site in *LAPTM5* 3′ UTR and mutated this poly(C) site (Fig. 5 *F* and *G*). The 3′ UTR of *LAPTM5*, but not antisense and mutated 3′ UTR, was associated with hnRNP K (Fig. 5*H*). Furthermore, EMSA showed that hnRNP K was able to bind to 3′ UTR of *LAPTM5* probes and failed to bind to mutated poly(C) probes (Fig. 5*I*). RIP assay revealed that OE of 3′ UTR but not OE of mutated 3′ UTR of *LAPTM5* remarkably increased the binding of hnRNP K (Fig. 5*J*). We also explored the binding domains of hnRNP K with *LAPTM5* using those mutants with the deleted KH domain (Fig. 2*K*). RIP assays showed that the KH3 domain of hnRNP K bound to *LAPTM5* (Fig. 5*K*). Overall, these data demonstrate that the poly(C) site in the 3′ UTR of *LAPTM5* directly interacts with the KH3 domain of hnRNP K.

***LCDR* Potentiates hnRNP K to Bind to and Stabilize *LAPTM5*.** Since both *LCDR* and hnRNP K regulate LAPTM5 expression, we then hypothesized that *LCDR* coordinates hnRNP K to bind to and stabilize the *LAPTM5* transcript. To verify this hypothesis, we first examined the endogenous *LAPTM5* mRNA level in the presence of actinomycin D, an inhibitor of transcription. Correspondingly, the stability of *LAPTM5* mRNA was significantly decreased in the *LCDR*-/hnRNP K–depleted cells or increased in the *LCDR*-/hnRNP K–overexpressed cells compared with each control cell (Fig. 6 *A* and *B*). Furthermore, the OE effects

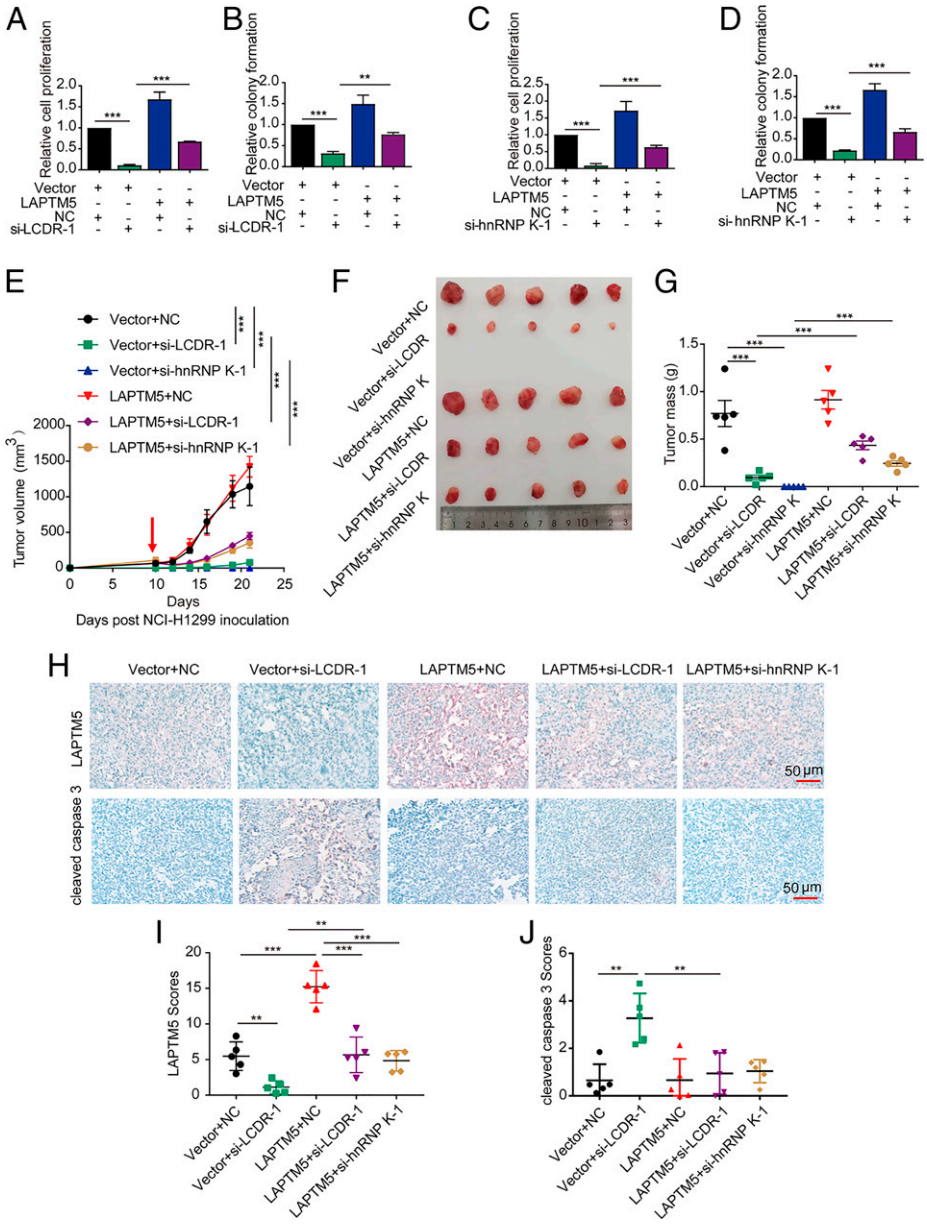

Fig. 4. *LCDR* and hnRNP K maintain cell survival through LAPTM5. (*A–D*) Relative cell proliferation (*A* and *C*) and colony formation (*B* and *D*) assays assessing NCI-H1299 cells expressing the indicated plasmids. Vector represents the empty vector as the OE negative control. (*E*) Effects of NCI-H1299 cells transfected with the indicated plasmids on tumor growth in subcutaneously implanted NSG mice. The same number of cells was injected into the recipient mouse on day 0 as baseline and formed measurable tumors on day 10 (red arrow). (*F* and *G*) Tumor size (*F*) and mass (*G*) in NSG mice subcutaneously implanted with NCI-H1299 cells transfected with the indicated plasmids ($n = 5$). (*H–J*) Representative images of LAPTM5 and cleaved caspase-3 and the quantification of signal intensities of tumor biospecimens from the above-mentioned xenografts ($n = 5$). NC, negative control. These data are presented as mean ± SD from three independent experiments. (Scale bars: 50 μm.) $^{**}P < 0.01$, Student's *t* test; $^{***}P < 0.001$, Student's *t* test.

of either hnRNP K or *LCDR* on the mRNA stability, mRNA, and protein levels of *LAPTM5* were completely abolished by KD of either *LCDR* or hnRNP K (Fig. 6 *A–D*). Given that both *LCDR* and hnRNP K located in the nucleus, we hypothesized that *LAPTM5* mRNA stability may occurs in the nucleus. The cellular fractionation assays revealed that *LAPTM5* transcripts were mainly expressed in the nucleus (*SI Appendix*, Fig. S14*A*). Furthermore, we explored the half-life of *LAPTM5* mRNA in the nucleus and cytoplasm. Strikingly, the *LAPTM5* mRNA stability was still significantly decreased in the nucleus of the *LCDR*-/hnRNP K–silenced cells compared with that of each control cells, while the stability of the cytoplasmic *LAPTM5* part was not changed (*SI Appendix*, Fig. S14 *B–E*). Correspondingly, the proportion of the cytoplasmic *LAPTM5* is significantly increased in *LCDR*-/hnRNP K–depleted cells (*SI Appendix*, Fig. S14 *F* and *G*). These results indicate *LCDR*/hnRNP K regulates *LAPTM5* stability in the nucleus, consistent with other studies that mRNA stability occurs in the nucleus (30, 31). Moreover, either *LCDR* or hnRNP K OE significantly increased the activity of the LAPTM5 3′ UTR reporter and failed to change the activity of the mutated LAPTM5 3′ UTR reporter (Fig. 6 *E* and *F*). These findings suggest that *LCDR* coordinates hnRNP K to mediate LAPTM5 expression by regulating its transcript stability.

LCDR KD remarkably decreased the binding of hnRNP K with *LAPTM5* (Fig. 6*G*), while *LCDR* OE, but not the *LCDR* mutant with the mutated poly(C) site, significantly increased interaction between hnRNP K and *LAPTM5* (Fig. 6*H*). Similarly, hnRNP K KD also remarkably reduced or OE of hnRNP K enhanced the association of *LCDR* with *LAPTM5* (Fig. 6 *I* and *J*). Moreover, protease K treatment completely abolished the interaction of LAPTM5 3′ UTR and *LCDR* (Fig. 6*K*). Altogether, these data indicate that *LCDR* enhances the binding ability of hnRNP K to *LAPTM5*.

As it was reported that the GXXG motif in the KH domain of hnRNP K is the key amino acid sequence to interact with the poly(C) site of RNA (19, 20) and since *LCDR* and *LAPTM5* bind to KH1 and KH3 domains of hnRNP K, respectively, we first constructed the two mutants with GXXG to GEEG conversions in either the KH1 or KH3 domain of hnRNP K (Fig. 6*L*). Next, we explored the effects of simultaneous co-OE of *LCDR*

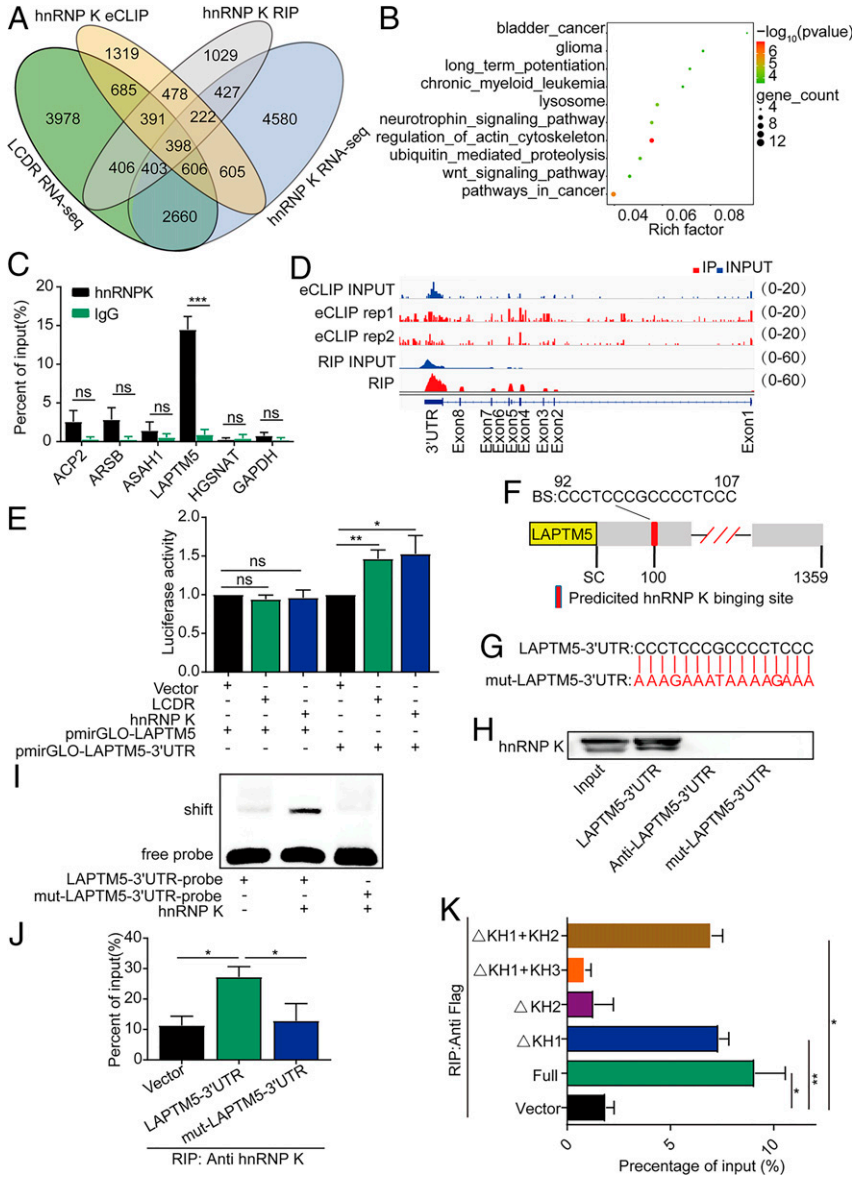

Fig. 5. *LAPTM5* directly binds with hnRNP K. (*A*) Venn diagram showing the overlapping genes by *LCDR* KD RNA-seq, hnRNP K KD RNA-seq, hnRNP K RIP-seq, and eCLIP-seq data. (*B*) The top 10 enriched KEGG pathways of the overlapping genes from *A*. (*C*) RIP assays showing enrichment efficiencies of hnRNP K with the indicated lysosome pathway genes in NCI-H1299 cells. (*D*) Distribution of hnRNP K peaks across the *LAPTM5* transcript based on hnRNP K RIP-seq and eCLIP-seq data. (*E*) The luciferase reporter assays showing *LAPTM5* 3′ UTR or CDS activity of NCI-H1299 cells with the indicated conditions. (*F* and *G*) Schematic diagram of the predicted hnRNP K BS in the *LAPTM5* 3′ UTR region (*F*) and mutated in this site (*G*). SC indicates stopping code. (*H*) RNA pull-down assays showing the association of hnRNP K with sense, antisense, and mutant of *LAPTM5* 3′ UTR. (*I*) EMSAs showing the interaction between hnRNP K and biotinylated LAPTM5 3′ UTR or mutant probes. (*J*) RIP assays showing the enrichment efficiencies of hnRNP K with *LAPTM5* in NCI-H1299 cells transfected with indicated plasmids. (*K*) RIP analysis for association of *LAPTM5* and hnRNP K in HEK293T cells transfected with the indicated plasmids from Fig. 2 *K* and *L*. eCLIP, enhanced cross-linking immunoprecipitation. IP, immunoprecipitation. ns, not significant. GAPDH, glyceraldehyde-3-phosphate dehydrogenase. RIP-seq, RNA immunoprecipitation sequencing. These data are presented as mean ± SD from three independent experiments. **P* < 0.05, Student's *t* test; ***P* < 0.01, Student's *t* test.

and hnRNP K on the binding of hnRNP K with *LAPTM5*. Consistently, the OE of either *LCDR* or hnRNP K enhanced the binding of *LAPTM5* with hnRNP K or luciferase expression of the *LAPTM5* 3′ UTR reporter (Fig. 6 *M* and *N*). However, cells with co-OE of both *LCDR* and hnRNP K showed significantly increased association of hnRNP K with *LAPTM5* or luciferase activity of *LAPTM5* 3′ UTR reporter compared with each OE (Fig. 6 *M* and *N*). As expected, such an effect was partially abrogated by co-OE of the hnRNP K KH1 mutant in combination with *LCDR*, indicating that KH1 mutation impaired the KH3 binding ability to endogenous LAPTM5. In contrast, the enhanced effect was completely diminished by co-OE of the hnRNP K KH3 mutant with *LCDR*, supporting that KH3 of the hnRNP K domain binds to *LAPTM5* (Fig. 6 *M* and *N*). Accordingly, EMSA showed that hnRNP K bound to *LCDR* and *LAPTM5* 3′ UTR at similar levels, but the binding ability of hnRNP K with *LCDR* and *LAPTM5* 3′ UTR probes was obviously potentiated (Fig. 6*O*), suggesting that *LCDR* and *LAPTM5* 3′ UTR may have synergistic binding to hnRNP K. Moreover, we designed a mixture of labeled/unlabeled equal probes to determine which probe enhanced binding with hnRNP K. Clearly, the enhanced effects of hnRNP K binding to probes was the labeled *LAPTM5* 3′ UTR probe but not the labeled *LCDR* probe (Fig. 6 *P*–*S*), suggesting that *LCDR* potentiates the binding ability of hnRNP K with *LAPTM5*. Altogether, these data demonstrate that *LCDR* binding to the KH1 domain of hnRNP K enhances the binding ability of the hnRNP K KH3 domain with *LAPTM5*, thus consequently increasing stability and expression of *LAPTM5*.

***LCDR* Is Up-Regulated and Targeting *LCDR* in Lung Cancer Patients.** To further explore the clinical relevance of these findings, we performed in situ hybridization (ISH) or IHC staining on a tissue microarray containing 98 lung adenocarcinoma (LUAD) and 82 pairs of matched adjacent tissues. ISH showed that *LCDR* mainly located in the nucleus, and IHC revealed that hnRNP K and LAPTM5 were expressed in the nucleus or cytoplasm, respectively (Fig. 7 *A*, *C*, and *E*). All of them were significantly up-regulated in LUAD tissues compared with the adjacent tissues (Fig. 7 *A*–*F* and Dataset S12). Further correlation analysis showed that *LCDR* expression was positively associated with the expression of either hnRNP K or LAPTM5, but the levels of hnRNP K were not correlated with LAPTM5 expression (*SI Appendix*, Fig. S15 *A*–*C*). In

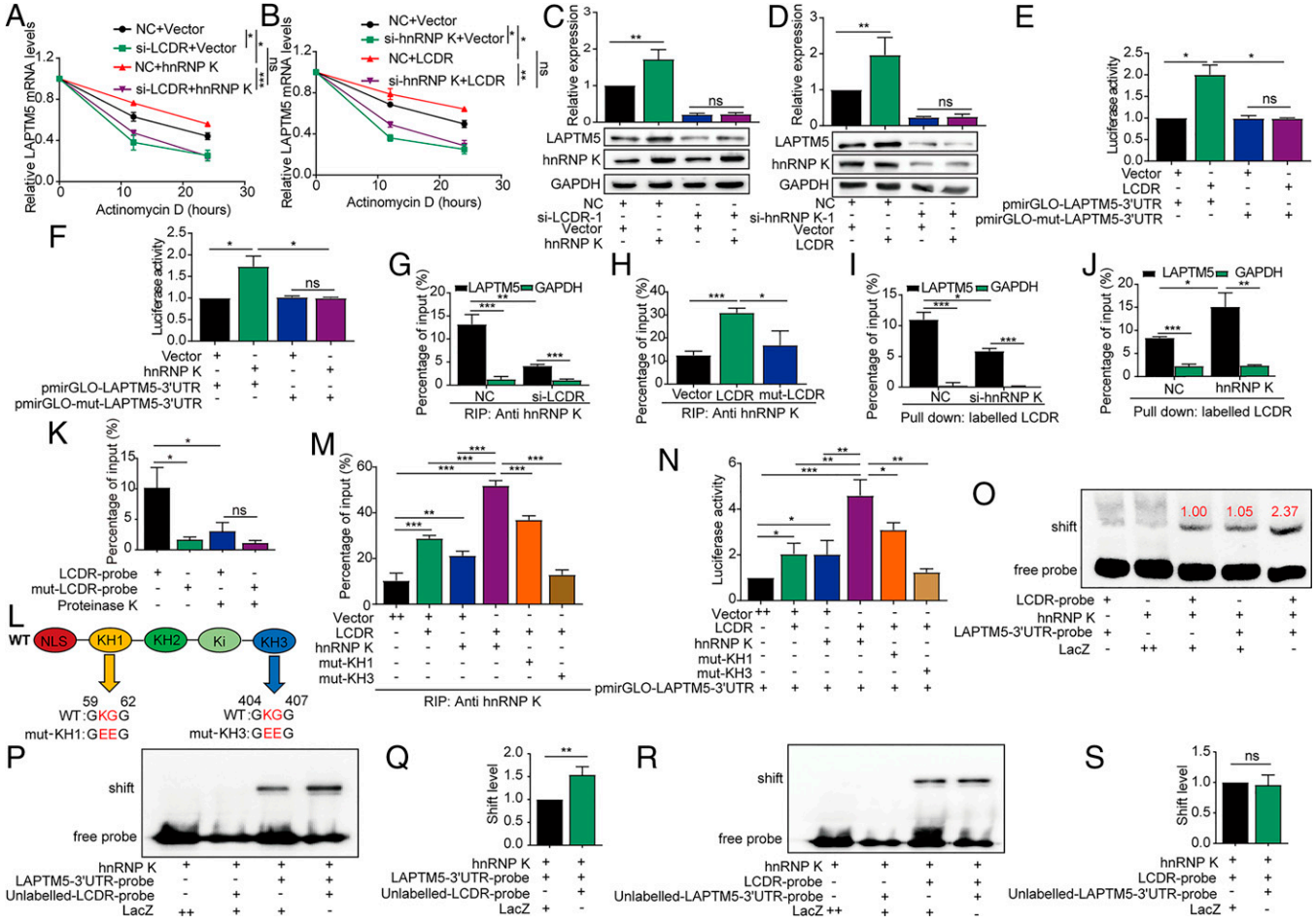

Fig. 6. *LCDR* potentiates hnRNP K binding to and stabilizing *LAPTM5*. (*A* and *B*) qRT-PCR analysis of the *LAPTM5* half-life after treatment with 5 μM actinomycin D for the indicated time in NCI-H1299 cells with indicated conditions. (*C* and *D*) qRT-PCR analysis of *LAPTM5* mRNA levels (*Upper*) and immunoblot analysis of LAPTM5 and hnRNP K (*Lower*) in NCI-H1299 cells. (*E* and *F*) The luciferase reporter assays assessing the *LCDR* (*E*) and hnRNP K (*F*) binding with *LAPTM5* 3′ UTR or mutant reporters. (Scale bar: 20 μm.) (*G* and *H*) RIP qRT-PCR detection of the enrichment of *LAPTM5* with hnRNP K in *LCDR* KD (*G*) and wild-type or mutant OE (*H*) in NCI-H1299 cells. (*I* and *J*) RNA pull-down assays showing the enrichment of *LAPTM5* with *LCDR* in the hnRNP K KD (*I*) and OE (*J*) NCI-H1299 cells. (*K*) RIP qRT-PCR detection of the enrichment of LAPTM5 with biotin-labeled *LCDR* or mut-*LCDR* RNA after treatment with or without protease K. (*L*) The schematic representation of the GXXG motif of the KH1 or KH3 domain of hnRNP K changed into GEEG. (*M* and *N*) RIP qRT-PCR assays showing the enrichment of *LAPTM5* with hnRNP K in HCI-H1299 cells (*M*) or the dual-luciferase reporter assays showing the luciferase activity of NCI-H1299 cells (*N*) transfected with the indicated plasmids. (*O*) EMSAs showing that the interaction between hnRNP K and *LCDR*, *LAPTM5* 3′ UTR, or LacZ probes. The numbers represent the relative intensities of shift bands quantified by ImageJ. (*P*–*S*) EMSAs showing the association of hnRNP K with the indicated labeled/unlabeled probes (*P* and *R*) and quantitative analysis of shift levels (*Q* and *S*). mut, mutation. GAPDH, glyceraldehyde-3-phosphate dehydrogenase. NLS, nuclear localization sequence. Ki, K-protein-interaction. WT, wild type. NC, negative control. These data are presented as mean ± SD from three independent experiments. ns, not significant, Student's *t* test. **P* < 0.05, Student's *t* test; ***P* < 0.01, Student's *t* test; ****P* < 0.001.

addition, receiver operating characteristic curve analysis showed that the expression combination of *LCDR*, hnRNP K, and LAPTM5 had increased sensitivity, specificity, and prediction to discriminate LUAD and normal tissues (*SI Appendix*, Fig. S15*D*). These findings highlight the important role of this axis in LUAD.

To regulate *LCDR* function and further evaluate its therapeutic potential in vivo, we designed a nucleus-targeting nanoplatform for si-*LCDR* delivery and evaluated its ability to inhibit tumor growth using the patient-derived xenograft (PDX) mice model. As a type of polyanionic biomacromolecule, siRNAs are easily attacked by serum nucleases and cannot readily cross the cell membrane and into nucleus (32). Thus, we designed an amphiphilic nucleus-targeting peptide (AUTP; $C_{17}H_{34}$-CONH-PKKKRKVRRRR-$CONH_2$), in which the PKKKRKV peptide could target the nucleus (33), while the RRRR peptide could complex siRNA via electrostatic interaction (34). After binding si-*LCDR*, the formed si-*LCDR*/AUTP complexes could be encapsulated into the hydrophobic core of the nanoparticles (NPs) made with an endosomal pH-responsive polymer, methoxyl-polyethylene glycol-*b*-poly (2-(diisopropylamino) ethylmethacrylate) (Meo-PEG-*b*-PDPA) (Fig. 7*G*). With this newly developed nanoplatform, it could rapidly respond to the endosomal pH to improve the endosomal escape ability of the encapsulated si-*LCDR* via the "sponge effect" (35). Subsequently, the exposed si-*LCDR*/AUTP complexes could specifically target the nucleus to achieve the goal of targeted delivery of si-*LCDR* for effective gene silencing in the nucleus (Fig. 7*G*). We first examined the physiochemical properties of the obtained nucleus-targeting nanoparticles (NT-NPs). These NT-NPs showed a well-defined spherical morphology with an average size of around 80 nm (*SI Appendix*, Fig. S16*A*). At an endosomal pH (e.g., pH 6.0), the protonation of the Meo-PEG-*b*-PDPA polymer could induce the disassembly of the NT-NPs, thereby leading to a faster release of the encapsulated si-*LCDR* compared with the NT-NPs incubated at pH 7.4 (*SI Appendix*, Fig. S16*B*). More importantly, after incubating the NT-NPs loading Cy5-labled si-*LCDR* with NCI-H1299

cells, these NPs could be internalized and escape from the endosomes (*SI Appendix*, Fig. S16*C*), which could then transport much more si-*LCDR* into the nucleus compared with control NPs made with the Meo-PEG-*b*-PDPA polymer and an amphiphilic cationic lipid-like compound without nucleus-targeting ability (*SI Appendix*, Fig. S16 *D* and *E*) (36). Therefore, these NT-NPs were ideally to assess the therapeutic efficacy and safety of siRNAs-targeted *LCDR* in the mouse model bearing PDXs.

Having validated the ability of the NT-NPs to improve the delivery of si-*LCDR* into the nucleus, we next evaluated whether the NT-NPs could employ this characteristic to enhance *LCDR* silencing. As expected, the NT-NPs si-LCDR-1 showed much stronger gene silencing efficacy compared with control NPs (*SI Appendix*, Fig. S17*A*). Correspondingly, NCI-H1299 cells with the NT-NPs si-LCDR-1 showed significantly decreased proliferation and colony formation (*SI Appendix*, Fig. S17 *B* and *C*) and enhanced apoptosis (*SI Appendix*, Fig. S17 *D–H*). In addition, immunoblot and immunofluorescence indicated that the level of LAPTM5 was dramatically reduced in the cells treated with the NT-NP si-LCDR-1 (*SI Appendix*, Fig. S17 *I* and *J*). Furthermore, immunofluorescence showed that LAMP1 and CTSB formed punctate staining patterns in phosphate-buffered saline (PBS) and control NPs cells, while they dissipated throughout the cytosol and showed no colocalization in NT-NPs si-LCDR-1 cells (*SI Appendix*, Fig. S17*K*). Collectively, these data demonstrate that NPs-mediated *LDCR* silencing results in LCD.

After confirming the efficient *LCDR* silencing and revealing the anticancer mechanism of NT-NPs si-LCDR-1, we next examined their pharmacokinetics (PK) and biodistribution (BioD). PK was examined by intravenous injection of NT-NPs loading Cy5-labeled si-*LCDR* to healthy mice. Due to the protection of the polyethylene glycol (PEG) outer layer, the NT-NPs showed longer blood circulation compared with naked si-*LCDR* (Fig. 7*H*). The BioD was examined by intravenous injection of NT-NPs loading Cy5-labeled si-*LCDR* to NSG mice bearing PDX from LUAD patients. With the long-circulating characteristic, the NT-NPs show much higher tumor accumulation than the naked si-*LCDR* (Fig. 7*I*). The tumors and major organs were harvested for BioD quantification, and results indicated that the accumulation of NT-NPs in the tumor tissues was around sixfold stronger than that of naked si-*LCDR* (Fig. 7*J* and *SI Appendix*, Fig. S18*A*). With the above promising PK and BioD results, we finally evaluated whether the NT-NPs could effectively knock down *LCDR* in vivo and promote antitumor effect. The NT-NPs were intravenously injected into the PDX-bearing mice once every 2 d at a 1-nmol siRNA dose per mouse. After three consecutive injections, compared with PBS and control NPs, the NT-NPs showed much stronger ability to inhibit the tumor growth (Fig. 7 *K–M*). The results of ISH and IHC staining further confirmed that the NT-NPs were the most effective to reduce the expression of *LCDR*, LAPTM5, and K_i-67 and induce apoptosis (Fig. 7 *N* and *O*). Notably, the administration of NT-NPs showed no obvious influence on mouse body weight (*SI Appendix*, Fig. S18 *B* and *C*). To further evaluate the potential in vivo side effects, the NT-NPs were intravenously injected into healthy mice (1-nmol siRNA dose per mouse, $n = 5$). After three consecutive injections, the levels of representative cytokines (tumor necrosis factor-α , interferon-γ, interleukin-6, and interleukin-12) were in the normal range (*SI Appendix*, Fig. S18 *D–G*). The blood routine analysis indicated that aspartate aminotransferase, alanine aminotransferase, albumin, blood urine nitrogen, creatinine, and total protein were in the normal ranges (*SI Appendix*, Fig. S18 *H–M*). In addition, histological analysis also showed no noticeable changes in the tissues of the heart, liver, spleen, lung, and kidney (*SI Appendix*, Fig. S18*N*). Collectively, these results indicate the low in vivo toxicity of NT-NPs developed in our work and that the use of NT-NPs for systemic si-*LCDR* delivery is an effective strategy for lung cancer treatment.

Discussion

Histone acetylation is one of the most common epigenetic modifications that regulates gene expression. In this study, we systematically mapped the HAR lncRNAs using TSA inhibitor in lung cells, which only inhibits the class I and II HDAC families but not class III HDACs, so this restricts the more broad-spectrum candidate lncRNAs to be identified (37). It has been shown that the expression of HDACs is aberrant and associated with poor outcomes in various cancer types (38–40), and targeting HDACs results to the inhibition of proliferation by inducing cell cycle arrest, differentiation, apoptosis, inhibiting angiogenesis, etc. in a series of cancer types (37, 41, 42). Targeting HDACs is a promising therapeutic strategy in cancer treatment; however, preclinical evidence shows that single-agent targeting of HDACs has only modest efficacy in cancer patient treatments (41, 43, 44), which may affect secondary signaling pathways being resistant to HDAC agents. As we find that TSA up-regulates *LCDR* expression in lung cancer cells and promotes cancer cell survival by maintaining lysosome integrity, this may contribute to resistance toward HDAC inhibitors. Clearly, our studies shed light on the molecular mechanism of targeting both lysosome and HDACs for future translational studies. Especially, the dysregulated expression of *LCDR* needs to be further investigated in future study.

RBPs play central roles in regulating gene expression, many of which are deregulated in various cancer types (11). Thus, RBPs are potentially attractive targets for cancer patient treatment, of which hnRNP K plays key functions as protumor or antitumor by regulating chromatin remodeling, transcription, and translation (15, 21, 22, 45). Also, numerous studies have shown that lncRNAs coordinate hnRNP K to promote or inhibit tumor progression, including neuroblastoma (46), hepatocellular carcinoma (47), and colorectal cancer (48), via the different signaling pathways. Herein, we showed that *LCDR* interacts with hnRNP K to promote lung cancer cell survival, may considering that this effect is not limited on lung cancer and is able to function on more broader tumor types. It has been shown that hnRNP K mediates resistance to apoptosis in tumor cells by regulating various mechanisms, such as transcription activation (21, 49) or alternative spicing of antiapoptotic genes (50, 51). Clearly, our study provides insight on hnRNP K–mediated apoptotic regulation and expands the knowledge of RBPs in regulation of cell death. This will improve our understanding of the mechanistic, functional, and pathological roles of hnRNP K in cancers and will contribute to therapeutic perspectives for cancer therapy.

Lysosomes maintain cellular homeostasis and contribute to cancer hallmarks, and targeting lysosome emerges as an attractive approach for cancer treatment. The dysregulated lysosome function, such as alteration of lysosomal composition, volume, cellular distribution, and enzyme activity, promotes cancer cell growth and survival (2), but the molecular regulation and underlying mechanism of lysosome remain poorly understood. *LCDR* is an lncRNA that maintains the intact lysosome and contributes to cancer cell survival. It has been shown that the transcriptional factor EB translocates into the nucleus, binds to the coordinated lysosomal expression and regulation motif, and regulates lysosome biogenesis at the transcriptional level (24). Furthermore, lysosome biogenesis requires the coordination of lysosomal protein biosynthesis and endosome–lysosome trafficking at translational and posttranslational levels (52). Herein, we verify that an *LCDR*/hnRNP K axis regulates lysosome by stabilizing the *LAPTM5* transcript, providing a mechanism of lysosome regulation at the posttranscriptional level. Inconsistent with our findings, LAPTM5 has been implicated in mediating LCD through

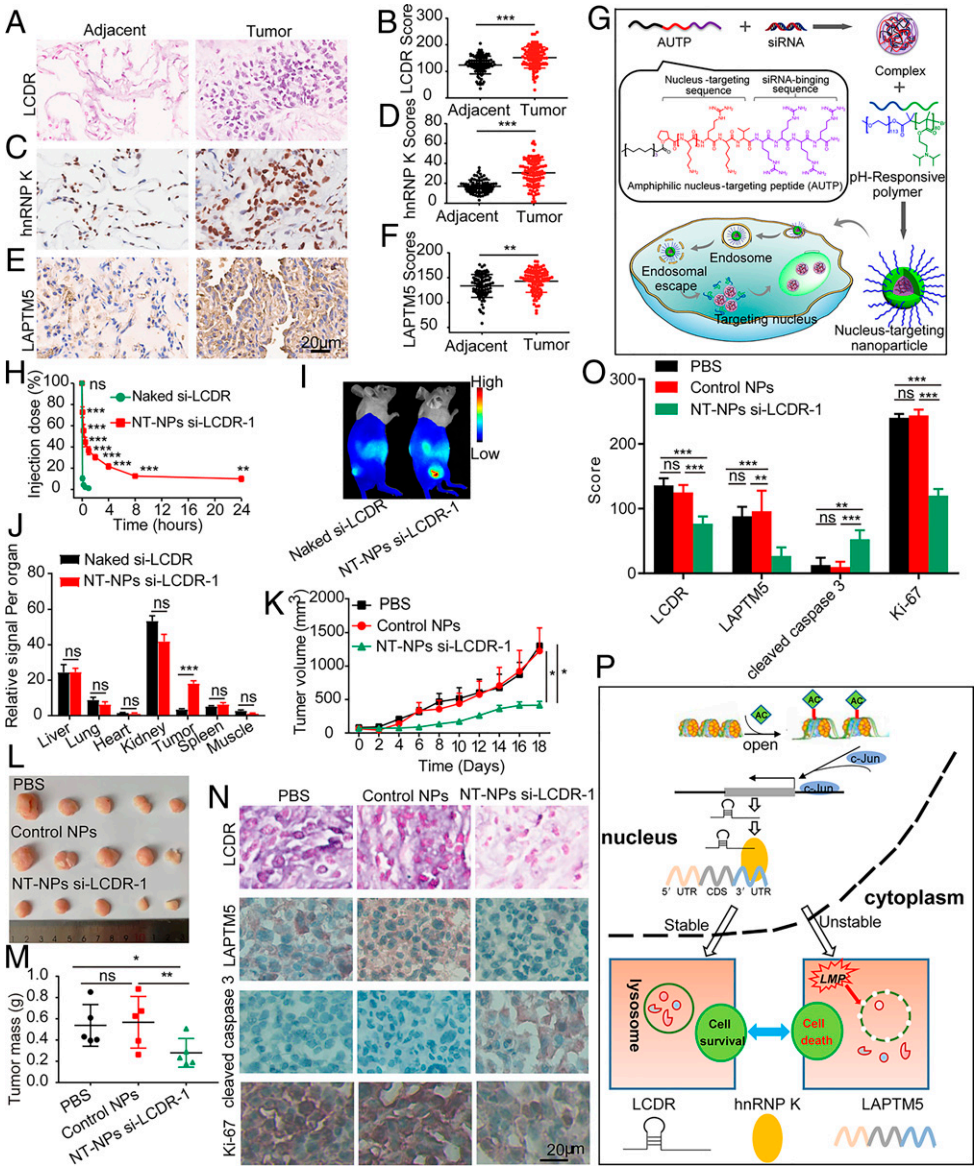

Fig. 7. The expression of *LCDR*, hnRNP K, and LAPTM5 in LUAD tissues and therapeutic potentials of *LCDR*. (*A*–*F*) Representative images and quantification of expression scores of *LCDR* (*A* and *B*), hnRNP K (*C* and *D*), and LAPTM5 (*E* and *F*) in LUAD tumor and adjacent tissues. (*G*) The schematic illustration of NT-NPs encapsulating siRNAs. (*H*) PK of naked si-LCDR and NT-NPs–si-LCDR-1 ($n = 3$). (*I*) Overlaid fluorescent image of the PDX-bearing mice postinjection of naked si-LCDR or NT-NPs–si-LCDR-1 after 24 h ($n = 3$). (*J*) BioD of naked si-LCDR and NT-NPs–si-LCDR-1 in the tumors and major organs of the PDX-bearing mice ($n = 3$). (*K*–*M*) Tumor growth curves (*K*), tumor images (*L*), and tumor weights (*M*) of the PDXs after treatment with PBS, control NPs, and NT-NPs–si-LCDR-1 ($n = 5$). (*N* and *O*) Representative images (*N*) and the quantification (*O*) of signal intensities of indicated molecules of tumor biospecimens in the above-mentioned PDXs. (Scale bar: 20 μm.) (*P*) Proposed model for the *LCDR*/hnRNP K/LAPTM5 axis promoting the survival of lung cancer cells. *LCDR*, which is activated by histone acetylation and transcribed by c-Jun, cooperates with hnRNP K to mediate *LAPTM5* expression by regulating its transcript stability, which keep the integrity of the lysosome membrane. Ki-67, Ki-67 protein. AC, acetylation. AUTP, amphiphilic nucleus-targeting peptide. Results are presented as the mean ± SD. ns, not significant, Student's *t* test. $*P < 0.05$; $**P < 0.01$; $***P < 0.001$.

destabilizing the lysosomal membrane in some tumor types/cell lines (53–55), which may be mediated by cell-type specificity, cellular-context dependence, or selection of the signaling pathway. The precise molecular and cellular mechanisms that resulted in inconsistency require further in-depth study. Moreover, the detailed link between LAPTM5 expression and LMP needs to be investigated using more models. Our study provided a proof of concept to employ NT-NPs for nucleus-targeting si-*LCDR* delivery to accomplish down-regulated LAPTM5 expression in vivo, suggesting a potential therapeutic target through LCD. Although the si-LCDR delivery system developed in this work could efficiently silence *LCDR* expression both in vitro and in vivo, it still has a long way to realize clinical translation. The main challenges include controllable NPs preparation and scalable manufacturing. In addition, the potential of long-term in vivo toxicity also needs to be systemically evaluated.

Overall, our data reveal that *LCDR* is an HAR protumorigenic lncRNA that mediates the integrity of lysosome by stabilizing hnRNP K–regulated *LAPTM5* in lung cancer (Fig. 7*P*). This study provides the underlying mechanism for lysosome regulation at the posttranscriptional level as well as the potential diagnostic and therapeutic targets for lysosome-targeted strategy.

Materials and Methods

Cell Lines and Clinical Specimens. The 293T, BEAS-2B, HCC827, Calu-1, and NCI-H1299 cells lines were obtained from the Shanghai Cell Bank Type Culture Collection Committee and cultured at 37 °C in a humidified incubator with 5% CO_2. The HCC827, Calu-1, and NCI-H1299 cell lines were cultured in RPMI-1640 medium (Gibco) supplemented with 10% fetal bovine serum (FBS). The 293T and BEAS-2B cells were cultured in Dulbecco's modified Eagle medium (DMEM) (Gibco) supplemented with 10% FBS. All cell lines were verified using short tandem repeat assays (Genetic Testing Biotechnology) and tested negative for mycoplasma contamination.

PDX Experiments. To establish PDXs, tumor specimens of lung cancer were collected from five patients who had been treated with at Sun Yat-Sen Memorial Hospital, Sun Yat-Sen University (Guangzhou, China) between 2021 and 2022. All five patients provided informed consent. The study was approved by the Institutional Review Board of Sun Yat-Sen Memorial Hospital, Sun Yat-Sen University. The procedure is described briefly below. Six-week-old NSG female mice were anesthetized by isoflurance. The tumors were minced into 1-mm^3-sized fragments and imbedded directly into the mammary fat pads. After the PDXs of the first generation reached diameters of 1 cm, they were harvested, minced into 1-mm^3-sized fragments, and imbedded directly into the mammary fat pads to establish the second generation for treatments. Each patient's PDX was transplanted into a mouse. Five PDX-carrying mice from

five patients were treated in each group. Tumor growth was monitored after transplantation using calipers. After the xenografts became palpable (around 150 mm^3), mice were intravenously injected with 1) NP–si-Lucifer and 2) NT-NPs–si-*LCDR* at a 1-nmol siRNA dose per mouse once every 2 d. After treatment for ∼3 wk, the mice were euthanized, and all the tumors were extracted and weighed. Furthermore, the tumor tissues were embedded in paraffin, sectioned, and stained with antibodies against LAPTM5 and cleaved caspase-3 according to previously reported protocols.

Additional methods can be found in *SI Appendix, SI Materials and Methods*.

Data Availability. HTML data have been deposited in Gene Expression Omnibus (accession no. GSE173849). All other data are included in the manuscript and/or supporting information.

ACKNOWLEDGMENTS. This work was supported by National Natural Science Foundation of China Grants 82025029, 81773023, 81874226, 82103230, and 81802526; Strategic Pilot Science and Technology Project Grant XDB29040103 and Scientific Research and Equipment Development Project Grant YJKYYQ20180032 of the Chinese Academy of Sciences; Technological Innovation Project of Shanxi Transformation and Comprehensive Reform Demonstration Zone Grant 2017KJCX01; and Key Research Project Grant 201903D321107 of Shanxi.

1. T. Kirkegaard, M. Jäättelä, Lysosomal involvement in cell death and cancer. *Biochim. Biophys. Acta* **1793**, 746–754 (2009).
2. S. M. Davidson, M. G. Vander Heiden, Critical functions of the lysosome in cancer biology. *Annu. Rev. Pharmacol. Toxicol.* **57**, 481–507 (2017).
3. D. Hanahan, R. A. Weinberg, The hallmarks of cancer. *Cell* **100**, 57–70 (2000).
4. D. Hanahan, R. A. Weinberg, Hallmarks of cancer: The next generation. *Cell* **144**, 646–674 (2011).
5. M. Huarte, The emerging role of lncRNAs in cancer. *Nat. Med.* **21**, 1253–1261 (2015).
6. F. P. Marchese, I. Raimondi, M. Huarte, The multidimensional mechanisms of long noncoding RNA function. *Genome Biol.* **18**, 206 (2017).
7. S. Gao *et al.*, DMDRMR-mediated regulation of m6A-modified CDK4 by m6A reader IGF2BP3 drives ccRCC progression. *Cancer Res.* **81**, 923–934 (2021).
8. A. M. Schmitt, H. Y. Chang, Long noncoding RNAs in cancer pathways. *Cancer Cell* **29**, 452–463 (2016).
9. X. Yang *et al.*, The long non-coding RNA PCSEAT exhibits an oncogenic property in prostate cancer and functions as a competing endogenous RNA that associates with EZH2. *Biochem. Biophys. Res. Commun.* **502**, 262–268 (2018).
10. Y. Gu *et al.*, *DMDRMR*-mediated regulation of m^6A-modified *CDK4* by m^6A reader IGF2BP3 drives ccRCC progression. *Cancer Res.* **81**, 923–934 (2021).
11. B. Pereira, M. Billaud, R. Almeida, RNA-binding proteins in cancer: Old players and new actors. *Trends Cancer* **3**, 506–528 (2017).
12. J. E. Audia, R. M. Campbell, Histone modifications and cancer. *Cold Spring Harb. Perspect. Biol.* **8**, a019521 (2016).
13. D. J. Hanly, M. Esteller, M. Berdasco, Interplay between long non-coding RNAs and epigenetic machinery: Emerging targets in cancer? *Philos. Trans. R. Soc. Lond. B Biol. Sci.* **373**, 373 (2018).
14. Z. Zhao, A. Shilatifard, Epigenetic modifications of histones in cancer. *Genome Biol.* **20**, 245 (2019).
15. Z. Wang *et al.*, The emerging roles of hnRNPK. *J. Cell. Physiol.* **235**, 1995–2008 (2020).
16. M. Zuker, Mfold web server for nucleic acid folding and hybridization prediction. *Nucleic Acids Res.* **31**, 3406–3415 (2003).
17. I. L. Hofacker, Vienna RNA secondary structure server. *Nucleic Acids Res.* **31**, 3429–3431 (2003).
18. A. V. Makeyev, S. A. Liebhaber, The poly(C)-binding proteins: A multiplicity of functions and a search for mechanisms. *RNA* **8**, 265–278 (2002).
19. H. Siomi, M. Choi, M. C. Siomi, R. L. Nussbaum, G. Dreyfuss, Essential role for KH domains in RNA binding: Impaired RNA binding by a mutation in the KH domain of FMR1 that causes fragile X syndrome. *Cell* **77**, 33–39 (1994).
20. Z. Yin *et al.*, RNA-binding motifs of hnRNP K are critical for induction of antibody diversification by activation-induced cytidine deaminase. *Proc. Natl. Acad. Sci. U.S.A.* **117**, 11624–11635 (2020).
21. Z. Xiao, H. L. Ko, E. H. Goh, B. Wang, E. C. Ren, hnRNP K suppresses apoptosis independent of p53 status by maintaining high levels of endogenous caspase inhibitors. *Carcinogenesis* **34**, 1458–1467 (2013).
22. J. Lu, F. H. Gao, Role and molecular mechanism of heterogeneous nuclear ribonucleoprotein K in tumor development and progression. *Biomed. Rep.* **4**, 657–663 (2016).
23. D. Tang, R. Kang, T. V. Berghe, P. Vandenabeele, G. Kroemer, The molecular machinery of regulated cell death. *Cell Res.* **29**, 347–364 (2019).
24. F. Wang, R. Gómez-Sintes, P. Boya, Lysosomal membrane permeabilization and cell death. *Traffic* **19**, 918–931 (2018).
25. M. E. Guicciardi, M. Leist, G. J. Gores, Lysosomes in cell death. *Oncogene* **23**, 2881–2890 (2004).
26. Y. Pak, W. K. Glowacka, M. C. Bruce, N. Pham, D. Rotin, Transport of LAPTM5 to lysosomes requires association with the ubiquitin ligase Nedd4, but not LAPTM5 ubiquitination. *J. Cell Biol.* **175**, 631–645 (2006).
27. M. Bogyo, S. Verhelst, V. Bellingard-Dubouchaud, S. Toba, D. Greenbaum, Selective targeting of lysosomal cysteine proteases with radiolabeled electrophilic substrate analogs. *Chem. Biol.* **7**, 27–38 (2000).
28. N. Malik *et al.*, The transcription factor CBFB suppresses breast cancer through orchestrating translation and transcription. *Nat. Commun.* **10**, 2071 (2019).
29. E. P. Consortium; ENCODE Project Consortium, An integrated encyclopedia of DNA elements in the human genome. *Nature* **489**, 57–74 (2012).
30. L. Fish *et al.*, Nuclear TARBP2 drives oncogenic dysregulation of RNA splicing and decay. *Mol. Cell* **75**, 967–981.e9 (2019).
31. A. Anantharaman *et al.*, ADAR2 regulates RNA stability by modifying access of decay-promoting RNA-binding proteins. *Nucleic Acids Res.* **45**, 4189–4201 (2017).
32. H. Yin *et al.*, Non-viral vectors for gene-based therapy. *Nat. Rev. Genet.* **15**, 541–555 (2014).
33. C. W. Pouton, K. M. Wagstaff, D. M. Roth, G. W. Moseley, D. A. Jans, Targeted delivery to the nucleus. *Adv. Drug Deliv. Rev.* **59**, 698–717 (2007).
34. S. M. Fuchs, R. T. Raines, Internalization of cationic peptides: The road less (or more?) traveled. *Cell. Mol. Life Sci.* **63**, 1819–1822 (2006).
35. X. Xu *et al.*, Ultra-pH-responsive and tumor-penetrating nanoplatform for targeted siRNA delivery with robust anti-cancer efficacy. *Angew. Chem. Int. Ed. Engl.* **55**, 7091–7094 (2016).
36. Z. Bi *et al.*, Nanoparticles (NPs)-meditated LncRNA AFAP1-AS1 silencing to block Wnt/β-Catenin signaling pathway for synergistic reversal of radioresistance and effective cancer radiotherapy. *Adv. Sci. (Weinh.)* **7**, 2000915 (2020).
37. R. W. Johnstone, J. D. Licht, Histone deacetylase inhibitors in cancer therapy: Is transcription the primary target? *Cancer Cell* **4**, 13–18 (2003).
38. W. Weichert *et al.*, Expression of class I histone deacetylases indicates poor prognosis in endometrioid subtypes of ovarian and endometrial carcinomas. *Neoplasia* **10**, 1021–1027 (2008).
39. W. Weichert *et al.*, Association of patterns of class I histone deacetylase expression with patient prognosis in gastric cancer: A retrospective analysis. *Lancet Oncol.* **9**, 139–148 (2008).
40. I. Oehme *et al.*, Histone deacetylase 8 in neuroblastoma tumorigenesis. *Clin. Cancer Res.* **15**, 91–99 (2009).
41. H. Mamdani, S. I. Jalal, Histone deacetylase inhibition in non-small cell lung cancer: Hype or hope? *Front. Cell Dev. Biol.* **8**, 582370 (2020).
42. D. M. Vigushin, R. C. Coombes, Targeted histone deacetylase inhibition for cancer therapy. *Curr. Cancer Drug Targets* **4**, 205–218 (2004).
43. T. Reid *et al.*, Phase II trial of the histone deacetylase inhibitor pivaloyloxymethyl butyrate (Pivanex, AN-9) in advanced non-small cell lung cancer. *Lung Cancer* **45**, 381–386 (2004).
44. Z. Jiang *et al.*, Tucidinostat plus exemestane for postmenopausal patients with advanced, hormone receptor-positive breast cancer (ACE): A randomised, double-blind, placebo-controlled, phase 3 trial. *Lancet Oncol.* **20**, 806–815 (2019).
45. M. Gallardo *et al.*, hnRNP K is a haploinsufficient tumor suppressor that regulates proliferation and differentiation programs in hematologic malignancies. *Cancer Cell* **28**, 486–499 (2015).
46. D. Li *et al.*, Long noncoding RNA pancEts-1 promotes neuroblastoma progression through hnRNPK-mediated β-catenin stabilization. *Cancer Res.* **78**, 1169–1183 (2018).
47. G. Qin *et al.*, Long noncoding RNA p53-stabilizing and activating RNA promotes p53 signaling by inhibiting heterogeneous nuclear ribonucleoprotein K deSUMOylation and suppresses hepatocellular carcinoma. *Hepatology* **71**, 112–129 (2020).
48. Z. Zhang *et al.*, Long non-coding RNA CASC11 interacts with hnRNP-K and activates the WNT/β-catenin pathway to promote growth and metastasis in colorectal cancer. *Cancer Lett.* **376**, 62–73 (2016).
49. L. C. Chen *et al.*, The antiapoptotic protein, FLIP, is regulated by heterogeneous nuclear ribonucleoprotein K and correlates with poor overall survival of nasopharyngeal carcinoma patients. *Cell Death Differ.* **17**, 1463–1473 (2010).
50. T. Revil, J. Pelletier, J. Toutant, A. Cloutier, B. Chabot, Heterogeneous nuclear ribonucleoprotein K represses the production of pro-apoptotic Bcl-xS splice isoform. *J. Biol. Chem.* **284**, 21458–21467 (2009).
51. A. Tyson-Capper, H. Gautrey, Regulation of Mcl-1 alternative splicing by hnRNP F, H1 and K in breast cancer cells. *RNA Biol.* **15**, 1448–1457 (2018).
52. C. Yang, X. Wang, Lysosome biogenesis: Regulation and functions. *J. Cell Biol.* **220**, e202102001 (2021).
53. J. Inoue *et al.*, Lysosomal-associated protein multispanning transmembrane 5 gene (LAPTM5) is associated with spontaneous regression of neuroblastomas. *PLoS One* **4**, e7099 (2009).
54. D. Y. Jun *et al.*, Ectopic overexpression of LAPTM5 results in lysosomal targeting and induces Mcl-1 down-regulation, Bak activation, and mitochondria-dependent apoptosis in human HeLa cells. *PLoS One* **12**, e0176544 (2017).
55. M. Nuylan, T. Kawano, J. Inazawa, J. Inoue, Down-regulation of LAPTM5 in human cancer cells. *Oncotarget* **7**, 28320–28328 (2016).